Computational Scaling Relationships Predict

Experimental Activity and Rate-Limiting Behavior

in Homogenous Water Oxidation

Daniel R. Harper^{1,2} and Heather J. Kulik^{1,*}

¹Department of Chemical Engineering, Massachusetts Institute of Technology, Cambridge, MA

02139

²Department of Chemistry, Massachusetts Institute of Technology, Cambridge, MA 02139

ABSTRACT: While computational screening with first-principles density functional theory (DFT) is essential for evaluating candidate catalysts, limitations in accuracy typically prevent prediction of experimentally relevant activities. Exemplary of these challenges are homogeneous water oxidation catalysts (WOCs) where differences in experimental conditions or small changes in ligand structure can alter rate constants by over an order of magnitude. Here, we compute mechanistically relevant electronic and energetic properties for 19 mononuclear Ru transition-metal complexes (TMCs) from three experimental water oxidation catalysis studies. We discover that 15 of these TMCs have experimental activities that correlate to a single property, the ionization potential of the Ru(II)-O₂ catalytic intermediate. This scaling parameter allows quantitative understanding of activity trends and provides insight into rate-limiting behavior. We use this approach to rationalize differences in activity with differing experimental conditions, and we qualitatively analyze the source of distinct behavior for differing electronic states in the other four catalysts. Comparison to closely related single-atom catalysts and modified WOCs enables rationalization of the source of rate enhancement in these experimental WOC catalysts.

Keywords: Ruthenium, density functional theory, water oxidation catalysts, scaling relations, catalytic conditions

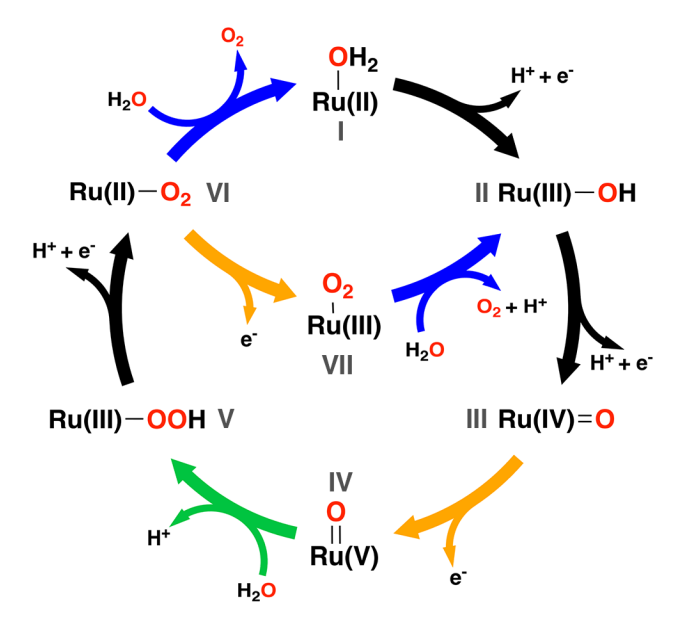
1. Introduction.

Improved catalysts are essential for meeting the goals of renewable energy, for instance in the production of renewable solar fuels through the water oxidation reaction. Homogeneous catalysts have attracted significant interest as water oxidation catalysts (WOCs) because the properties of transition-metal complexes (TMCs) can be finely tuned though ligand modification.²⁻⁴ Water oxidation has been demonstrated at a single metal site in a TMC^{5,6}, motivating efforts to optimize their catalytic properties. Experimental efforts to determine the ligands compatible with water oxidation⁷⁻⁹ or identify design criteria for more active WOCs¹⁰⁻¹⁴ have often consisted of trial-and-error synthesis of a set of TMCs and measurement of their activity.⁷⁻¹⁴ This approach has led to significantly improved homogeneous WOCs, the most active of which contain Ru metal centers. 15,16 However, many of these improved catalysts rely on through-space interactions¹⁶⁻¹⁹ such as pendant bases^{18,19} to achieve an increase in catalytic activity. Ligand modifications that improve catalytic activity via through-bond effects are desirable, because they are more robust to changes in reaction conditions, and also provide a complementary approach to increasing activity. Rational WOC design would benefit from firstprinciples modeling, but changes in activity either due to subtle ligand variation or modification of experimental conditions can be challenging to predict a priori. As a result, demonstrations of first-principles ligand design have only been recent and limited in scope.²⁰

A number of mechanisms for water oxidation have been proposed. We focus on the water nucleophilic attack (WNA)²¹ mechanism, which is thought to be responsible for the most active catalyst identified thus far¹⁶ (Scheme 1). Although there is strong support for the WNA mechanism, water oxidation is also believed to be possible via the dimerization of two metal-oxo units.²²⁻²⁴ Experimental methods have revealed specific details of this mechanism,²⁵⁻²⁷ but

accurate computational modeling is expected to be critical to gain a more complete understanding of the intermediates and competing pathways.²⁸ The WNA mechanism has been characterized computationally,^{29,30} with particular emphasis on the electronic structure and reactivity of the high-valent Ru(V)=O species,³¹⁻³³ the O₂ release step,³⁴ and photoisomerization.³⁵ However, it is not yet known which fundamental properties predict catalytic activity, a key piece of information for computationally guided design.

Scheme 1. The water nucleophilic attack (WNA) mechanism for water oxidation. Steps are colored based on the type of each reaction. Oxygen dissociation is shown in blue. Proton-coupled electron transfer steps (PCET) are shown in black. Electron transfer steps are colored yellow. The key O–O bond formation step is shown in green.



Computation is an effective tool for accelerating the discovery of novel catalysts,^{36,37} but it is necessary to obtain accurate properties which correlate to experimentally measured catalytic activity. Many ligand modifications are thought to function by changing the identity of the rate-determining step in water oxidation catalysis.³⁸⁻⁴² These ligand designs have included oxygen atom transfer to a pendant base,³⁹ nucleophilic attack by a carboxylate group,^{40,41} and additional elementary steps related to reversible changes in ligand conformation.⁴² The ability of the precise

rate-determining step within the WNA framework to be tuned is typical of homogeneous catalysis⁴³⁻⁴⁵ and computation has been essential in identifying this variability.⁴⁶⁻⁴⁸ While changes in mechanism and catalytic activity can be quantified directly through microkinetic modelling⁴⁹ or through formalisms such as the degree of rate control^{50,51} or the energetic span model^{52,53}, direct prediction of experimental rates remains challenging.

While more frequently exploited in heterogeneous catalysis⁵⁴⁻⁵⁶, linear correlations (i.e. scaling relationships) can simplify catalyst screening, an approach which has been demonstrated fruitfully on related metal—organic frameworks,^{57,58} single-atom catalysts,^{59,60} and homogeneous systems.⁶¹⁻⁶³ Further, scaling relationships predict the relative activity of catalysts, which benefits from cancellation of some of the systematic error⁶⁴ present in density functional theory (DFT)⁶⁵⁻⁶⁹ and particularly in TMCs.^{65,70-72} While universal scaling relationships for WOCs have been proposed,^{73,74} recent work (e.g., in C–H activation) suggests⁷⁵⁻⁷⁸ that scaling relationships in homogeneous catalysis need to be tailored for specific ligand types⁷⁹ and should account for the influence of reaction conditions.⁴⁵

In this work⁸⁰, we compare the computed properties of a set of closely related homogeneous WOCs to previously reported rate constants from three experimental studies (Figure 1 and Supporting Information Table S1).^{8,12-14} To demonstrate the utility of scaling relationships for reducing errors in computational catalyst screening, we select only WOCs which are thought to be active via the WNA mechanism, avoid through-space interactions with the catalytic intermediate, and contain a ruthenium metal center. Even then, the set of catalysts we study have different absolute and relative experimental rates as a result of distinct conditions in each study (Figure 1 and Supporting Information Table S1).^{8,12-14} As a result, we must both develop independent scaling relations to explain these differing experimental results and also

devise an approach to confirm comparable electronic structure across the catalysts being compared. For the homogeneous catalysts obtained from these experimental data sets, we propose a metric for identifying similar and dissimilar electronic states. We demonstrate that effective scaling relationships can be constructed for catalysts with similar electronic states, but that these do not readily extend to all WOCs. We show that our scaling parameter accurately predicts the relative activity of catalysts within these closely related TMCs and that different slopes in these scaling relations prevail when experimental conditions are varied.

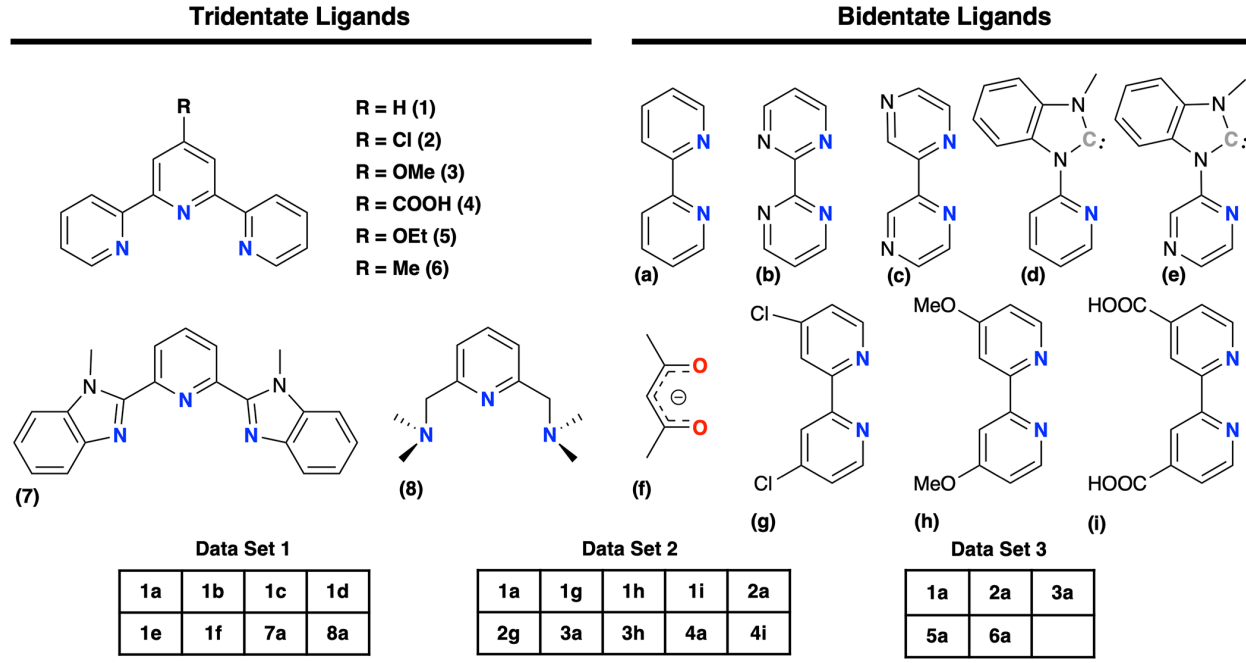


Figure 1. The 19 TMCs considered in this work from three literature sources, data sets 1⁸, 2¹², and 3^{13,14}. Each TMC consists of a ruthenium metal center complexed with a tridentate ligand (left) and a bidentate ligand (right). Experimentally measured rate constants for the water oxidation reaction are available for each TMC, from at least one of three literature sources (i.e., where each source tested multiple catalysts under the same experimental conditions), as indicated in the grid at bottom.

2. Computational Details.

All geometry optimizations and single-point calculations were performed using density functional theory (DFT) and a developer version of TeraChem v1.9.81,82 The B3LYP83-85

functional was employed with the LANL2DZ⁸⁶ effective core potential for Ru and the 6-31G* basis set⁸⁷ for all elements. This modest basis set choice is justified by recent observations⁸⁸ that trends in relative energetics of ionization energies and spin-state dependent properties from this basis set are of equivalent quality to larger triple- ζ (i.e., def2-TZVP) basis sets. Similarly, it is known that it is challenging to model triplet O_2 accurately with generalized gradient approximations⁵⁵, but a focus on relative energetics has motivated our calculation of properties involving O_2 intermediates (e.g., ligand dissociation energies) in our catalytic cycle as has been previously carried out.^{30,89}

Solvent corrections, ΔG_{solv} , were added using the conductor-like polarizable continuum implicit solvent model^{90,91} implemented^{92,93} in TeraChem with a dielectric constant of 80. Singlet calculations were carried out in a spin-restricted formalism, while all other calculations were spin unrestricted, and the lowest-energy spin multiplicity is always reported for each intermediate (Supporting Information Table S2 and Figure S1). Level shifting was applied with the virtual orbitals shifted by 0.25 Ha.⁹⁴ Geometry optimization in translation rotation internal coordinates⁹⁵ using the L-BFGS algorithm were carried out on molecules in implicit solvent. Default geometry optimization convergence thresholds of 4.5 x 10⁻⁴ Ha/bohr and 10⁻⁶ Ha were used for the gradient and change in the total energy between steps, respectively. For each optimized geometry, we computed the Hessian to confirm the absence of any imaginary frequencies and to obtain energy corrections for the zero-point energy and vibrational entropy at a temperature of 300 K. Entropic terms from other (i.e., rotational, translational, and electronic) degrees of freedom were neglected. We made this choice because the double-ζ calculations were efficient with GPUaccelerated quantum chemistry in TeraChem and force field pre-optimization with molSimplify, but an alternative approach would have been to use semi-empirical structures in a hierarchical

scheme⁹⁶⁻⁹⁸, as has been recently proposed for WOCs.⁹⁹ Population analysis was carried out with an interface between TeraChem and Natural Bond Orbital analysis (NBO) v6.0.²

Initial structures for each unique TMC and each intermediate of the WNA catalytic cycle were either generated using molSimplify¹⁰⁰⁻¹⁰² which uses OpenBabel^{103,104} as a backend or by modifying a previously converged structure (Supporting Information Table S3). As in prior work, the successful completion of each calculation was judged based on two criteria. First, the final structure was required to pass a series of geometric health checks to ensure that the calculation converged to the expected octahedral geometry as introduced in prior work (Supporting Information Table S4). For all open-shell calculations, the deviation from the expected value of $\langle S^2 \rangle$ (i.e., S(S+1)) was required to be less than a 1 μ B² cutoff for spin contamination, established in prior work (Supporting Information Table S5). As described previously and validated against correlated wavefunction theory benchmarks of, this cutoff ensures that only cases where spin states differ by at least one unpaired electron from the expected value are excluded.

In this work, we developed strategies to recover jobs that failed to pass the $\langle S^2 \rangle$ check or for which the self-consistent field (SCF) calculation failed to converge. For spin-contaminated cases, the geometry optimization was attempted with the fraction of Hartree–Fock (HF) exchange set to 0% (i.e. BLYP). For cases with SCF failures, level-shifting values were adjusted to 1.0 Ha for the majority-spin virtual orbitals and 0.1 Ha for the minority-spin virtual orbitals. When these recovery strategies were successful in addressing the original failure, their final structures and wavefunctions were used as inputs to a new geometry optimization using the B3LYP (i.e., 20% HF) functional and the original level-shift values of 0.25 Ha (Supporting Information Table S6).

To validate our choice of DFT functional, we compared results to B3LYP with modified amounts of HF exchange (i.e., (0–30% in increments of 5%) and three range-separated hybrid functionals, CAM-B3LYP, ¹⁰⁷ ωB97X, ¹⁰⁸ and LRC-ωPBEh¹⁰⁹ (Supporting Information Text S1). We observed the linear correlation between computed Gibbs energy values and experimentally measured benchmarks to be insensitive to functional choice, with the linear correlation comparable (*R*²: 0.84–0.90) regardless of the functional selected (Supporting Information Figure S2). Although direct simulation of external oxidant has recently been attempted in modeling of WOCs¹¹⁰, we do not explicitly model the external oxidant and instead add -1.6 VSHE to steps involving oxidation to avoid challenges of DFT in accurate treatment of highly charged systems. ⁶⁸ We expect that since the chemical structures of the catalysts in this work are all roughly comparable, the explicit modeling of the oxidant would not significantly alter trends reported in this work. However, explicit modeling of oxidant could be useful if more varied catalyst structures were evaluated in the future.

Three types of properties were calculated in order to capture trends in the WNA mechanism that could predict the overall rates of the experimentally measured catalytic cycle. We calculated the Gibbs energy of reaction, ΔG , at pH = 0 (i.e., to reflect the acidic conditions common in experiments) and 300 K for each step while incorporating corrections for zero-point vibrational energy, entropy, and the solvation environment. The energetics of the rigid ligand dissociation energy, ΔE_{LD} , of oxygen from the Ru(II)-O₂ and Ru(III)-O₂ intermediates as well as the vertical ionization potential, ΔE_{IP} , of the Ru(II)-O₂ and Ru(IV)=O intermediates were determined based on single-point calculations (Supporting Information Text S2). The calculation of ΔE_{LD} and ΔE_{IP} neglected the corrections for zero-point vibrational energy and entropy. This approximation was motivated by the nearly constant (std. dev. < 1 kcal/mol) value of these

corrections in the computation of ΔE_{LD} (Supporting Information Table S7).

3. Results and Discussion.

3a. Energetics of a Representative WOC.

We first focus on TMC 1a, a well-known WOC^{5,8,12-14,21,30,31,34}, to quantify baseline reaction energetics (Figure 1). As 1a was among the first mononuclear WOCs discovered⁵, it is included in all of the experimental data sets considered in this work and is expected to be broadly representative of TMCs that catalyze the WNA mechanism (Scheme 1). The 1a structure contains motifs common among most of the catalysts in this work (Figure 1). Specifically, the 1a structure has an octahedral coordination geometry with nitrogen atoms from tridentate and bidentate ligands that coordinate the metal in a way that constrains ligating atom positions (Figure 1). The WNA mechanism that 1a participates in is believed to include three proton-coupled electron transfer (PCET) steps,¹¹¹ two electron transfer steps, one of two possible O₂ dissociation steps, and an O–O bond formation step, which can each have different degrees of control over overall catalytic activity (Scheme 1).

To determine potential rate-limiting steps in the WNA catalytic cycle, we computed the reaction coordinate for TMC **1a** (Figure 2). For each PCET step, the reaction is exergonic when we account for an oxidant (e.g., Ce(IV))¹² with a redox potential of 1.6 V,¹¹² suggesting these steps are unlikely to be rate limiting. Nevertheless, it has been suggested¹¹³ that the potential limiting step may not necessarily be the same as the rate determining step. In comparison, the other two electron transfer steps, Ru(IV)=O to Ru(V)=O and Ru(II)-O₂ to Ru(III)-O₂, require 0.67 eV and 0.15 eV, respectively, even after accounting for an oxidant (Supporting Information Table S8 and Figure S3). For the two O₂ dissociation steps, we note that each is included in a different possible reaction pathway (Scheme 1). Because which pathway dominates is influenced

by the rate of electron transfer from Ru(II)-O₂, either O₂ dissociation step has the possibility of being overall rate-limiting step. Water exchange with Ru(II)-O₂ becomes more competitive when an external oxidant is not accounted for in the energetics (Supporting Information Figure S3). Finally, the O–O bond formation step is strongly exergonic (i.e., $\Delta G = -1.06$ eV) in the presence of external oxidant, but this thermodynamic favorability does not guarantee favorable kinetics *a priori* (Supporting Information Table S8 and Figure S3). After eliminating the three PCET steps as candidate rate-limiting steps based on our calculations, the remaining options, i.e., two electron transfer steps, the O–O bond formation step, and two possible O₂ dissociation steps, are consistent with those that have been identified as rate limiting in experimental studies.^{8,14,21,31} Alternative treatment of PCET steps has been proposed (i.e., direct from III to V)¹¹⁴, but considering that would not change our conclusions.

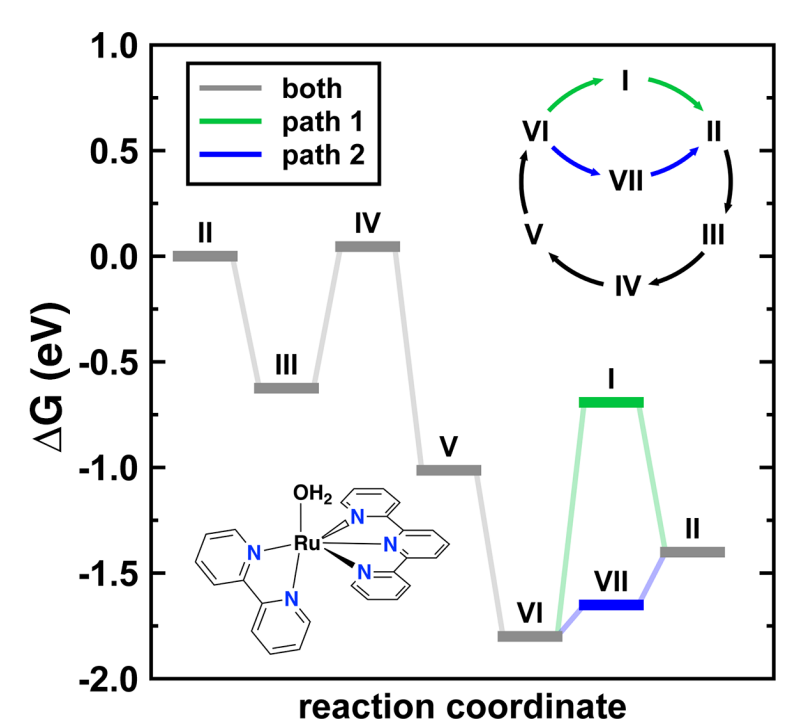


Figure 2. Energetics of the WNA catalytic cycle for TMC **1a**. The labeling of intermediates is shown inset (top right) and corresponds to the catalytic cycle shown in Scheme 1. For steps involving the transfer of an electron (I to II, II to III, III to IV, V to VI, and VI to VII), we add **1.6** eV to the step's energetics to account for the presence of an external (i.e., Ce(IV)) oxidant. Energetics are shown for both the reaction path where O₂ directly dissociates (green) and the

path where an electron transfer precedes O_2 dissociation (blue). For most intermediates, the two paths are identical (gray).

To aid interpretation and accelerate screening, we identify electronic properties that we can easily compute with DFT, are related to each of the five candidate rate-limiting steps, and thus could correlate with the overall experimentally measured reaction rate. To avoid explicit calculation of time-consuming transition states, we rely on the Bell-Evans-Polanyi (BEP) principle 115,116 and compute quantities related to reaction free energies, ΔG . We compute the Gibbs energy to complete a full catalytic cycle accounting for external oxidant, which we refer to as ΔG WNA. Additionally, to model the rate of O–O bond formation or electron transfer steps, we use the DFT-computed ΔG of these steps. For the two O₂ dissociation steps, we compute only the rigid ligand dissociation energy, $\Delta E_{\rm LD}$, of O_2 , which provides an upper bound on the energetics of O₂ dissociation. In addition to BEP relations, Marcus theory¹¹⁷ suggests that the kinetics of electron transfer processes should be related to vertical ionization potential, $\Delta E_{\rm IP}$ (Supporting Information Table S9 and Text S3). We thus also compute the $\Delta E_{\rm IP}$ for both electron transfer steps, bringing to seven the number of DFT properties that could capture catalytic activity (Supporting Information Table S10). This approach contrasts with computational scaling relations typically derived for heterogeneous catalysts that instead focus on adatom adsorption energies.

3b. Electronic Structure Similarity Defines a Subset of WOCs.

The electron configuration of a molecular WOCs is expected to influence its catalytic activity¹¹⁸, limiting our ability to understand and predict differences in activity from geometric structure and chemical composition alone. To detect distinct electron configurations among the catalysts in our data set, we quantified differences based on the population of localized natural

bond orbitals (see Computational Details). Using the closed-shell singlet Ru(II)-OH₂ intermediate, we collected the occupations of orbitals that localized to the 5s and 4d subshells of Ru(II) (i.e., six orbitals) or to the 2s and 2p subshells of the axial-coordinating O atom (i.e., four orbitals) into a 10-dimensional feature vector. Visualization of the first two principal components (95% of the variance) from principal component analysis (PCA) indicates that the 19 TMCs cluster into three distinct groups, with the largest group containing most (i.e., 15) of the TMCs (Figure 3 and Supporting Information Figure S4). These three groups are consistently present if alternate intermediates are chosen for analysis, although more overlap between groups is observed for the oxidized (i.e., Ru(IV)=O/Ru(V)=O) species (Supporting Information Figure S5).

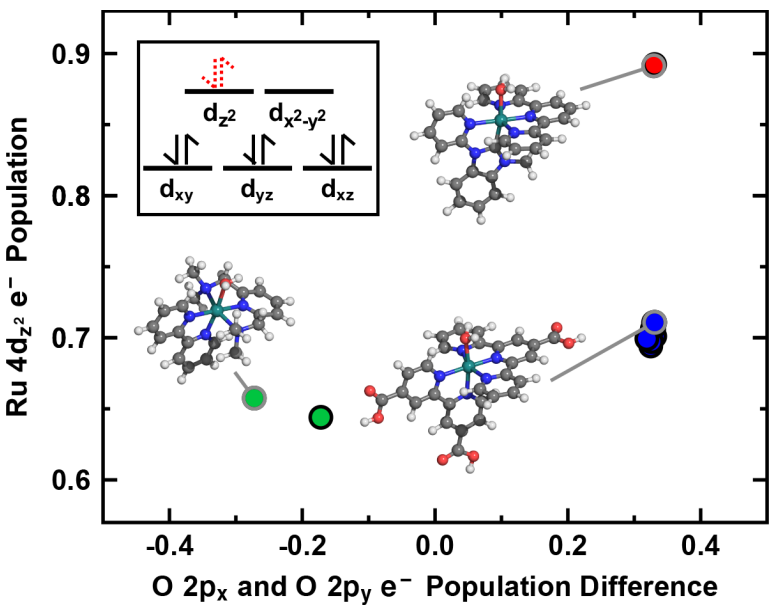


Figure 3. Plot of the natural orbital populations for intermediate **I** that distinguish electronic states of the 19 TMCs studied: difference between the O $2p_x$ and $2p_y$ orbital populations vs Ru d_z^2 orbital total population. Fifteen catalysts (blue circles) have qualitatively similar populations, and smaller clusters have enhanced d_z^2 populations (red) or distinct relative occupation in the p orbitals (green). Insets illustrate representative structures, and an electron configuration diagram provides a cartoon of the formal electron configuration (black solid arrows) and distinguishes which states are differentially populated for catalysts in the red cluster (red dashed arrows).

Relative to the majority cluster, the differences in the other clusters can largely be

attributed to either the Ru $4d_z^2$ or O $2p_x/2p_y$ orbitals, as the occupations of the remaining seven orbitals are nearly constant (Figure 3 and Supporting Information Table S11). Specifically, one cluster has additional electron density (ca. 0.2 e^-) in the Ru $4d_{z^2}$ orbital, whereas electron density (ca. 0.3 e^-) shifts from the oxygen $2p_x$ to the $2p_y$ orbital in the other cluster (Supporting Information Table S11). It may at first be surprising that a formally d^6 metal center has significant occupancy in the d_z^2 orbital, but this can be attributed to bonding interactions between the metal and water. When electrons are shared, they will lead to occupancy in orbital populations, even if the metal is oxidized. For the more oxidized intermediates (i.e. Ru(III)-OH, Ru(IV/V)=O, and Ru(III)-OOH), there is naturally less distinction between this second group and the 15-TMC majority group (Supporting Information Figure S5).

Because we expect scaling relationships to hold most optimally when similar electronic states are compared, we focus our analysis of the relationship between DFT and experimental properties to this subset. For these 15 TMCs, most of the DFT properties are well correlated ($R^2 > 0.85$) with each other, indicating that a single scaling relationship likely applies for all properties (Figure 4). The four electron transfer properties correlate positively to each other but negatively to the ΔG of the O–O bond formation step and ΔE_{LD} for Ru(II)-O₂ (Supporting Information Figure S6). The single uncorrelated property, ΔE_{LD} of O₂ from Ru(III), does not correlate well with other steps in part because it is uniformly small (ca. 6 kcal/mol) for all catalysts in our data set (Figure 4 and Supporting Information Table S10). Because Ru(III)-O₂ ΔE_{LD} is an upper limit for ligand dissociation, we conclude it is unlikely to be rate limiting over these 15 TMCs and exclude it from further consideration. Notably, dissociation of O₂ estimated by Ru(III)-O₂ ΔE_{LD} is lower than that for Ru(II)-O₂ because differences in the spin states (i.e., singlet vs doublet) and electron configuration lead to a longer initial Ru-O bond length by over

0.1 Å on average (Supporting Information Table S10 and see Supporting Information .zip file).

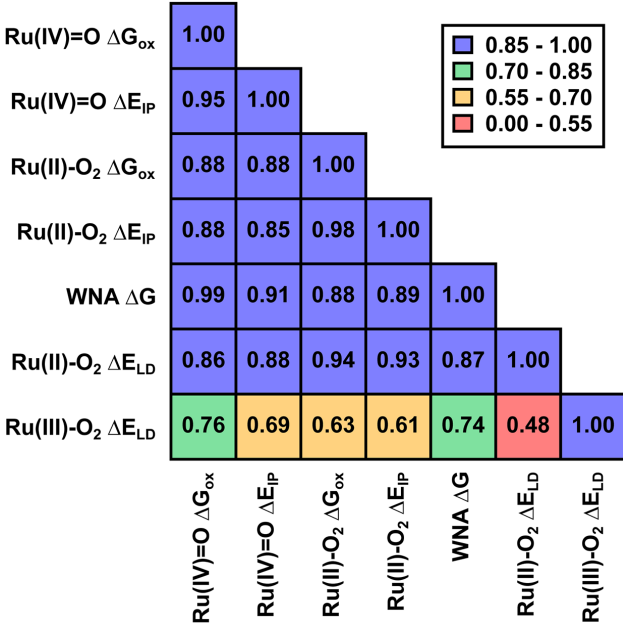


Figure 4. Coefficient of determination (R^2) between seven pairs of quantities calculated using DFT that might be expected to influence catalytic activity. Six of the parameters are well correlated to each other (blue, $R^2 > 0.85$), as indicated by the numerical values and colors in the inset legend.

Overall, most correlations are intuitive, e.g., a higher Ru(IV)=O ΔE_{IP} corresponds to more favorable WNA (i.e., because the WNA ΔG is expected to be more favorable for a more stable Ru(IV)=O), whereas others, e.g., the negative correlation between ΔE_{IP} and ΔE_{LD} in Ru(II)-O₂, are less obvious (Supporting Information Table S12). While such correlations may not hold across a broader set that has greater structural or chemical diversity, they suggest consistent reactivity trends should be observable over the 15 TMC subset of molecular WOCs obtained from the three distinct experimental data sets. Overall, this analysis suggests a single scaling parameter can be used to estimate relative catalyst activity from DFT, whereas if the correlations were weaker, it would mean that tuning one property may have inconsistent effects on different portions of the catalytic cycle. We select Ru(II)-O₂ ΔE_{IP} as this scaling parameter because it has the largest average correlation (R^2 : 0.86) and requires only a single geometry optimization to

compute (Figure 4). The applicability of a single property to describe a full catalytic cycle is well established in both heterogeneous or homogeneous catalysis, but direct calculation of ionization potentials is not straightforward in the solid state where frontier orbital energies have instead been favored.

Since all descriptors correlate similarly well, the analysis carried out can be expected to be invariant to the choice of descriptor, and in solid state water oxidation, a focus on a step that does not involve change in formal charge (e.g., Ru(II)-O₂ ΔE_{LD}) may instead be preferred. Additionally, some of our descriptors involve relaxation of multiple intermediates (i.e., ΔG WNA), but they correlate just as well to the vertical ionization potentials we have selected. As we also optimize intermediates in multiple oxidation states, we can compare the adiabatic ionization potential to the vertical ΔE_{IP} . For the representative case of **1a**, the Ru(IV)=O ΔE_{IP} is 0.1% lower than the adiabatic IP while Ru(II)-O₂ ΔE_{IP} is 4% lower. These relative magnitudes can be rationalized by the slight increase in Ru-O bond observed for Ru(III)-O₂ (see Supporting Information). Similarly, adiabatic ligand dissociation energies are within 1 kcal/mol of the rigid dissociation energies, which can be expected due to limited change in the catalyst structure with O₂ binding (see Supporting Information).

3c. Thermodynamic Properties Predict Activity.

After having shown that the seven DFT properties that we expect to influence catalytic activity are correlated to each other, our primary goal now is to determine if our chosen scaling parameter also correlates to experimentally measured rate constants. Differences in rate constants even for the same catalyst due to differences in conditions experimentally means that we cannot obtain a single fit through all of the data (Supporting Information Table S1).^{8,12-14} Instead, we focus on obtaining a best-fit line for each of the catalysts in the three experimental studies that

belong to the 15 TMC subset. After distinguishing the catalyst subsets and pruning to the 15 TMC subset, predicted rate constants, based on a best-fit line with the B3LYP Ru(II)-O₂ $\Delta E_{\rm IP}$. match experimental rates to within a factor of three in all cases (Figure 5 and Supporting Information Tables S13-S14). This good performance (i.e., beyond typical hybrid DFT accuracy) is due to error cancellation possible only because we have curated a set of catalysts with comparable geometry and electronic structure. TMC 7a in experimental data set 1 is the only outlier in this analysis, with first-order dependence on oxidant concentration in its rate law whereas all other catalysts in this subset are zero-order in oxidant, preventing direct comparison to our descriptor on an equal footing. This is somewhat expected, as the 1.78 eV value of the Ru(II)-O₂ ΔE_{IP} descriptor for this catalyst is the lowest in data set 1 and on the lower end for the majority cluster of 15 TMCs (Supporting Information Tables S10–S11). For large changes in the descriptor such as this, we expect commensurate changes to the rate of underlying elementary steps, potentially influencing which step is rate limiting. Even though we have taken steps to ensure consistency of the electronic structure for the complexes studied, our approach is not immune to changes in the identity of the rate-limiting step. This change in rate law could also mean that TMC 7a may evolve O₂ via an alternate reaction mechanism (e.g., I2M with a catalyst dimer). For example, the sacrificial oxidant Ce(IV) ammonium nitrate has also been reported to be involved in capturing and releasing O-O containing species. 120 Nevertheless, we included 7a in our study because it was present in experimental data set 1, and the goal of the present work is to determine the extent to which computational descriptors can predict experimental activity.

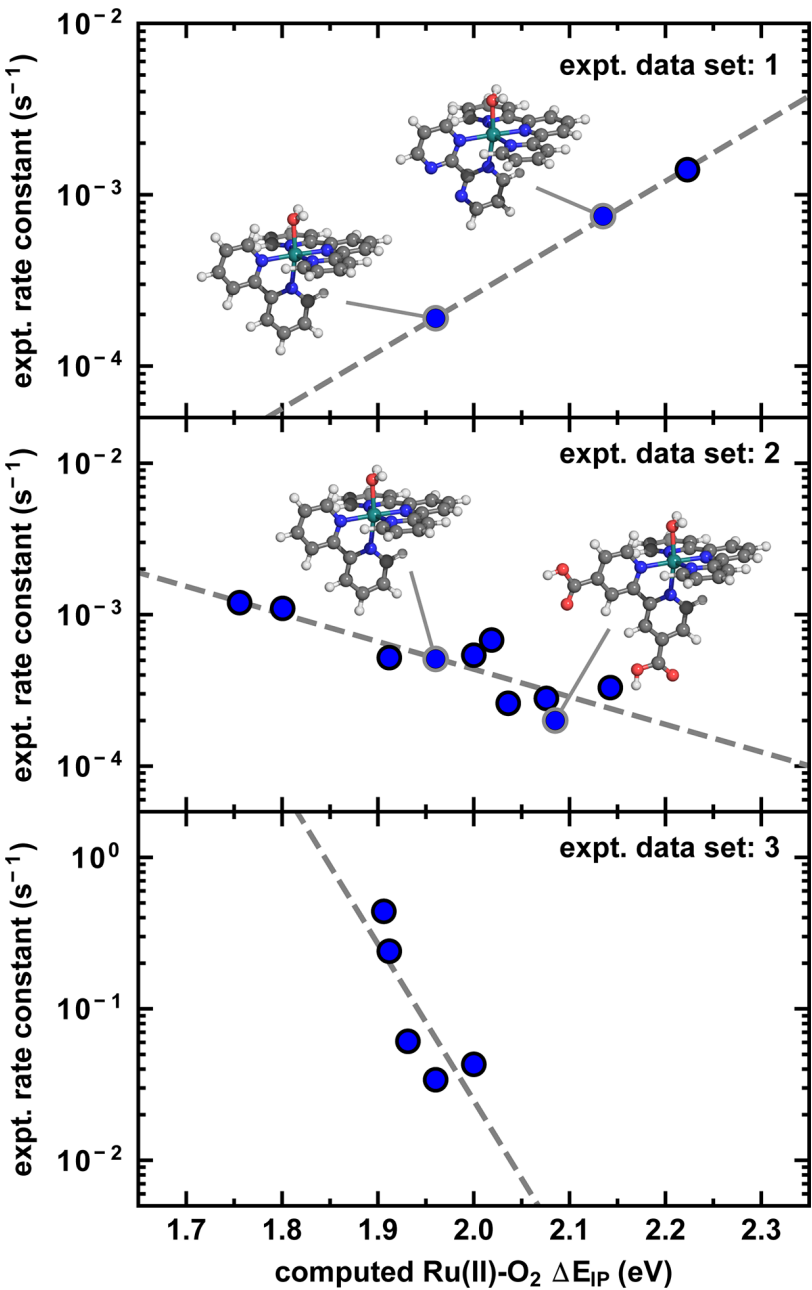


Figure 5. The experimentally measured rate constant (s⁻¹) vs the computationally derived scaling parameter, Ru(II)- $O_2 \Delta E_{IP}$, (in eV). The data is separated based on the source of the experimental data, as indicated in the inset label in each pane. The Ru(II)- OH_2 intermediates of the **1a** and **1b** TMCs are shown as insets in data set 1, and **1a** and **1i** are shown as insets in data set 2 in ball-and-stick representation colored as: C in gray, O in red, N in blue, H in white, and Ru in teal. One catalyst (**7a**) from data set 1 has a second-order rate law and thus the rate constant cannot be visualized on this plot.

We have established that only a subset of the data fits a single scaling relationship with our DFT-based descriptors, and within each experimental set, different best-fit lines are observed due to differences in experimental conditions and measured rates even for the same catalyst structure (Figure 5). Thus, we can use the slope of the correlation between our descriptor and experimentally measured rate constant to interpret possible differences in rate-limiting steps with a change in experimental conditions. Computationally determined volcano plots are one way to reduce to a single dimension the trade-offs between competing steps. Here, our approach differs slightly because we are comparing similar tuning effects on catalyst structures but under distinct conditions. Based on this analysis, we conclude that the rate-limiting step in data set 1 is either O₂ dissociation or O–O bond formation, both of which become more energetically favorable as our descriptor increases (Supporting Information Table S12). In stopped-flow kinetic experiments, ligand dissociation was assigned as the rate-limiting step for these catalysts, consistent with our observation.²¹ Nevertheless, since we have only three data points that we correlate in data set 1, more data would be useful to corroborate this observation. A potential limitation of the present work is that we cannot guarantee the $\Delta E_{\rm IP}$ descriptor will be useful to predict the activity of catalysts for which experimental rate constants are not known and for which another state (e.g., PCET in WNA) could be the rate determining step.

Conversely, in experimental data sets 2 and 3, one of the electron transfer steps could be rate limiting, as these become more favorable as the descriptor decreases (Supporting Information Table S12). We hypothesize these differences in rate-limiting steps derive from differences in reaction conditions across experiments. For example, the concentration of oxidant (Ce^{IV}) was 30 equivalents in experimental data set 1 and only qualitative excess in data sets 2 and 3 (Supporting Information Table S1).^{8,12-14} This additional oxidant potentially activates path 2 for O₂ release (i.e., by oxidation first to Ru(III)-O₂), enabling the catalyst to circumvent slower O₂ dissociation from Ru(II)-O₂. Electrochemical data might be easier to correlate than those with

external oxidants, but in the present work we specifically aimed to rationalize and study differences in reported experimental data sets based on external oxidant choices. An alternative explanation for the observed differences between the data sets with differences in oxidant concentration is that the oxidant may not be in true excess but instead is required for an additional step for O₂ release via one electron oxidation (i.e., as in pathway 2).

We can understand the effect of changes in rate-limiting steps on trends in catalytic activity by examining two additional representative TMCs (i.e., **1b** and **1i** along with **1a**). Both are differentiated from **1a** by the addition of peripheral electron-withdrawing groups that increase (by 0.12-0.17 eV) the Ru(II)-O₂ ΔE_{IP} scaling parameter (Figure 5). In data set 1, this modification (i.e., **1a** to **1b**) increases catalytic activity by nearly threefold (295%) due to more favorable dissociation of dioxygen from Ru(II)-O₂. This observation is alternatively consistent with our descriptor-based analysis indicating that O–O bond formation is more favorable. In data set 2, the similar modification (i.e., **1a** to **1i**) decreases catalytic activity (by 61%) due to the decreasing favorability of electron transfer steps (Supporting Information Table S13). Therefore, modifications to the catalyst that would result in increased activity under one set of reaction conditions can lead to diminished activity under different reaction conditions.

3d. Understanding the Activity of Dissimilar WOCs.

In comparison to the 15 TMCs with similar electronic structure, there is experimental evidence⁸ that the other four catalysts do not share the same rate-limiting step. Instead of zero-order dependence on the oxidant concentration, experimental rates for three out of four remaining TMCs are first-order in oxidant. The rate order of the fourth TMC, **1f**, can be either zero- or first-order in oxidant depending on the progress of the reaction (Supporting Information Table S1). While the experimental rate appeared correlated to properties relevant to O₂

dissociation or O–O bond formation for the other catalysts from data set 1 (see Sec. 3c), the dependence of the rate on oxidant concentration suggests that the slowest step may involve electron transfer for these outlier TMCs. While we already noted that a shift in the Ru(II)-O₂ $\Delta E_{\rm IP}$ descriptor (1.39–1.89 eV) in comparison to the majority TMCs (1.96–2.22 eV) can influence the rate law, this analysis suggests that a change in the catalyst's preferred electronic state can also alter the identity of the slowest step in the catalytic cycle.

Unsurprisingly, the developed scaling relationships between computational properties that applied to the 15 TMCs does not simultaneously apply to the four outlier TMCs (Supporting Information Figure S7). While for the 15 TMCs, deviations from scaling relations of energetic properties were small (ca. 0.5 kcal/mol), large deviations (ca. 4 kcal/mol) are observed when predicting the O–O bond formation and O₂ dissociation (i.e., WNA ΔG and Ru(II)-O₂ ΔE_{LD}) energetics of the outlier TMCs. Intermediate deviations (ca. 2 kcal/mol) are observed for prediction of the electron transfer steps (e.g., Ru(IV)=O ΔE_{IP}) for these four catalysts (Supporting Information Table S15). While the Ru(II)-O₂ ΔE_{IP} scaling parameter explains relative catalyst performance among 15 TMCs with similar electronic states in similar experimental conditions, it does not generalize across multiple electron configurations. While additional scaling relations could be built for these outlier catalysts, it would likely require more data (i.e., more than four catalysts) than is available from these three experimental sets.

Because quantitative analysis of the outlier catalysts is challenged by differences in rate order and scaling relations, we instead carry out a qualitative assessment. We focus on the Ru(II)-O₂ ΔE_{IP} versus Ru(II)-O₂ ΔE_{LD} scaling relationship that applies to the 15 TMCs for the majority cluster but from which the outlier TMCs deviate strongly (Figure 6 and Supporting Information Figure S7). For the TMCs with increased $4d_z^2$ orbital occupation (i.e., 1d and 1e),

Ru(II)-O₂ $\Delta E_{\rm LD}$ values are lower (ca. 7 kcal/mol) than expected from the scaling relationship, suggesting more rapid O₂ dissociation (Figure 6 and Supporting Information Table S15). We would therefore expect increased catalytic activity and rate-limiting electron transfer. Consistent with our expectations, **1d** and **1e** were approximately two orders of magnitude more active than **1a** in the original experimental study.⁸ The decreased Ru(II)-O₂ $\Delta E_{\rm LD}$ in **1d** and **1e** is likely due to the strong σ -donor ligand that can be expected to reduce the barrier to O₂ dissociation via the trans effect (Figure 1).

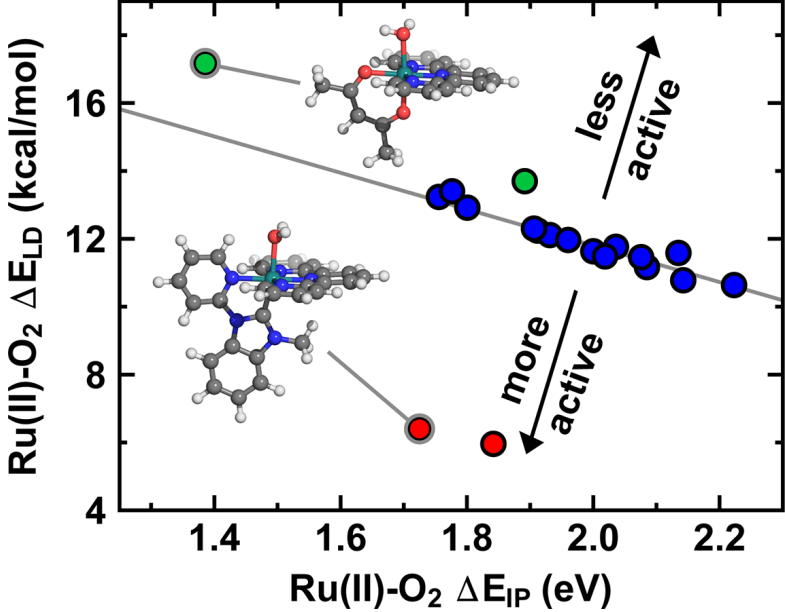


Figure 6. Ru(II)-O₂ ΔE_{IP} (in eV) vs Ru(II)-O₂ ΔE_{LD} (in kcal/mol) for the majority cluster of 15 TMCs (blue circles) through which a best-fit line (gray) is shown. Four TMCs excluded from the fit are colored according to whether they have an increase in Ru d_z² occupation (red circles) or shifted relative O 2p_x and 2p_y occupations (green circles). Representative Ru(II)-OH₂ intermediates are shown in ball-and-stick representation and colored by element as: carbon in gray, nitrogen in blue, hydrogen in white, oxygen in red, and ruthenium in teal.

For the other two catalysts with shifted O $2p_x$ and $2p_y$ occupations (i.e., **1f** and **8a**), Ru(II)-O₂ ΔE_{LD} is instead increased (ca. 2 kcal/mol) relative to the scaling relationship (Figure 6, Supporting Information Table S15). Although this analysis might lead us to conclude that these two catalysts should undergo slower O₂ dissociation and have lower overall catalytic activity,

experiments suggest they are both two orders of magnitude more active than 1a.⁸ This discrepancy can be rationalized by noting multiple paths for oxygen dissociation are possible in the WNA mechanism (Scheme 1). Because O₂ dissociation from Ru(II)-O₂ is somewhat less favorable for these TMCs without an observed decrease in activity, O₂ dissociation from Ru(III)-O₂ could instead be favored.

3e. Ligand Rigidity Improves Catalytic Activity.

All of the experimental catalysts studied in this work contain rigid multidentate ligands common among homogeneous Ru WOCs. To understand why this motif has emerged in this class of catalyst, we investigate the effect of lifting such constraints on catalyst energetics. By constructing lower-denticity, monodentate analogues of the ligands in the multidentate **1a** WOC, we isolate the effect of conformational flexibility (Figure 7 and Supporting Information Table S16). First, we note that both standard **1a** and its unconstrained form have fairly consistent reaction energetics (i.e., within 0.2 eV) for all but one step. The exception is the oxidation of Ru(IV)=O to form Ru(V)=O, which is less favorable in the unconstrained TMC by 0.53 eV, suggesting rigidity is essential for stabilizing Ru(V)=O in TMC **1a**.

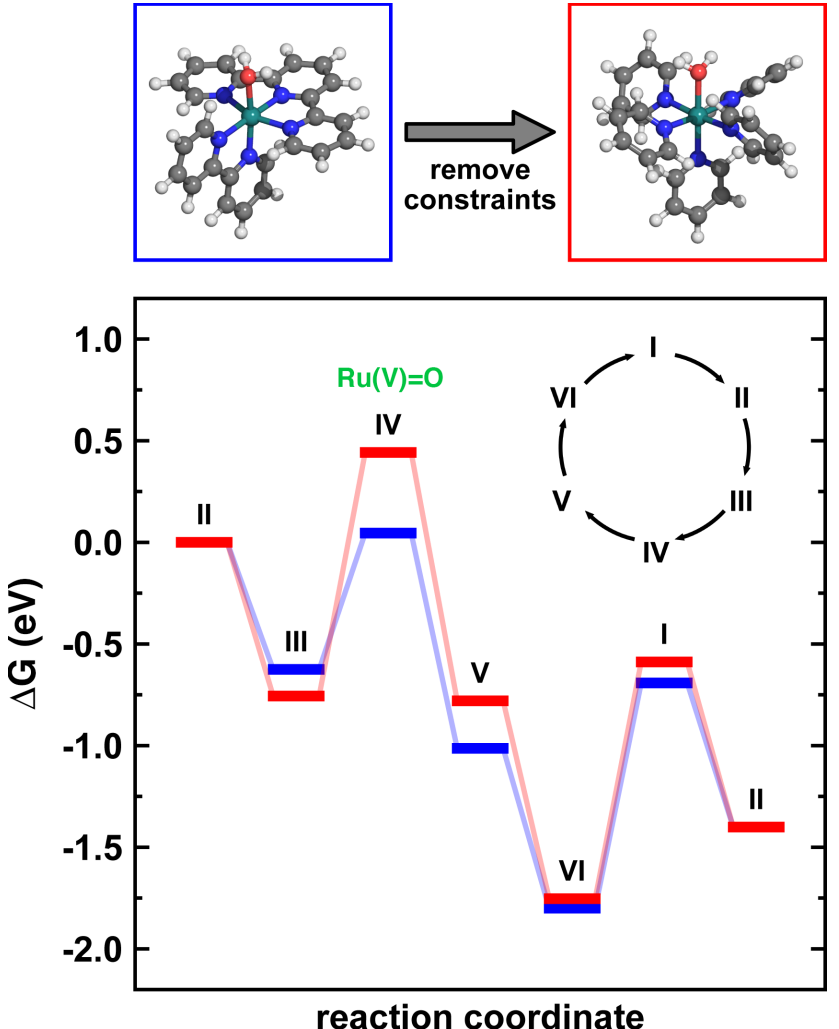


Figure 7. Comparison of energetics of the WNA catalytic cycle (in eV) when the TMC ligands are conformationally constrained (blue) or unconstrained (red). Inset structures (top) show the bonds that are removed to construct an unconstrainted equivalent. Each step is identified as an intermediate labeled between I and VI, with the labels matching the intermediates in Scheme 1, and the Ru(V)=O intermediate is also annotated in green. The alternative pathway 2 (intermediate VII) has been omitted for clarity due to the similarity of closely related, reduced VI for both constrained and unconstrained SACs.

Given the emerging relevance of N-doped graphene single-atom catalysts (SACs)⁵⁹ as a heterogeneous analogue to molecular catalysts for oxidation³⁷, we also investigated whether rigidity plays a role in the increased activity of SACs. We constructed a minimal SAC model, consisting of Ru in a planar tetradentate structure reminiscent of an N-doped graphene sheet with a distal axial water, as well as a monodentate, unconstrained form of the SAC model (Supporting

Information Figure S7 and Table S16). When the denticity is reduced in the flexible model, we observe a similar shift (by 0.52 eV) upward of the energetics for Ru(IV)=O oxidation to form Ru(V)=O, suggesting the effect of rigidity is indeed general (Supporting Information Table S17). Another role that the rigid ligands could be playing is in reducing steric hindrance to the binding axial moiety (Figure 7). Thus, we expect that rigidity in homogeneous WOCs or graphitic SACs will play a key role in stabilizing the key Ru(V)=O intermediate for the WNA mechanism to lead directly to O–O bond formation. While the benefit of the rigid nature of N-doped graphitic SACs and its molecular mimics is well established^{37,59,121,122}, there have been cases of enzyme mimic WOCs (i.e., cubanes) where monodentate ligands that enable dynamic rearrangement have instead been preferred.¹²³ Thus, while our observations of beneficial rigidity are outside the margin of error in the hybrid DFT calculations, they cannot necessarily be extended to all WOCs.

To predict the activity of the graphene SAC for water oxidation, we make qualitative comparisons to those of the 15 experimental TMCs but do not expect it to follow the same scaling relationship as the majority set of TMCs due to differences in electronic state and coordination. For five of the seven properties we identified to influence catalytic activity, the rigid (i.e., standard) SAC model properties reside within the range of values obtained on the 15 TMCs (Supporting Information Tables S10 and S16). For the other two properties, i.e., $\Delta E_{\rm LD}$ and $\Delta E_{\rm IP}$ of the Ru(II)-O₂ intermediate, the SAC properties are significantly less favorable. The $\Delta E_{\rm LD}$ of 20 kcal/mol is significantly higher (10–13 kcal/mol in the 15 TMCs) and the Ru(II)-O₂ $\Delta E_{\rm IP}$ of 2.5 eV is also increased (1.8–2.2 eV in the 15 TMCs). These observations suggest that this SAC model is unlikely to efficiently catalyze a WNA mechanism because it disfavors both O₂ dissociation from Ru(II)-O₂ and formation of an Ru(III)-O₂ intermediate. Rather, SAC activity

for water oxidation using Ru¹²⁴ or other metals^{122,125-127} is likely the result of a modified mechanism involving an additional oxygen atom¹²⁴ or components of the extended SAC material that have an influence beyond rigidity alone. Future work could further delineate the extent to which differences in SACs are due to rigidity or differences in the electronic state, for example by repeating the rigidity analysis on **1a** and by carrying out principal component analysis on both the SACs and molecular catalysts.

4. Conclusions.

Small changes in catalyst structure and/or reaction conditions can lead to significant changes in catalytic rates in a manner that is challenging to predict from first principles. We demonstrated an approach to building scaling relationships between efficiently computed first-principles (i.e., with DFT) properties and experimentally measured rates across three studies of water oxidation catalysts. First, using a representative WOC, we identified the most likely rate-limiting steps in the WNA catalytic cycle and computed several properties that correlated both to each other and the key steps in WNA. From the relative activity of experimentally characterized WOCs obtained from three different experimental studies reported in literature, we identified the ionization potential of a Ru(II)-O₂ intermediate to correlate well to the majority of catalyst activities across these experimental studies.

Because catalysts with distinct electronic structure could not be expected to follow the same scaling relationships, we devised a strategy for distinguishing the electronic state favored by the catalyst based on the electron population in the natural bond orbitals of the metal center and axial oxygen atom. Using this metric, we confirmed that 15 of the TMCs had similar electron configurations for the Ru(II)-OH₂ intermediate, whereas two TMCs had increased electron density in the $4d_z^2$ orbital of the ruthenium center and two TMCs had electron density

shifted from the 2p_x to the 2p_y orbital of oxygen. Across the studies where correlations could be obtained between experiment and computed properties, the slope of the correlation could be used to infer whether the experimental rate-limiting step of the reaction was O₂ dissociation, O–O bond formation, or electron transfer. While by design we used experimental data sets with differing conditions to understand real world challenges when comparing results from different sources, future steps could focus on reducing these sources of uncertainty. For example, in some cases, the 2,2'-bipyridine ligand (bidentate a in Scheme 1) in the TMCs have been reported¹² to dissociate or undergo oxidation in reaction conditions. While most cases (i.e., except 7a from source 1⁸) this ligand fit our correlations, further examination of our study could identify if it should be excluded in future scaling relation analysis.

While scaling relationships do not easily generalize quantitatively to WOCs with distinct electronic states, qualitative inferences about the activity of possible TMCs were possible based on the sign of deviations from the scaling relationships. These observations motivated predictions of the role of rigidity in a Ru complex with more flexible ligands and a Ru SAC analogue. This approach reveals properties that govern the activity of homogeneous WOCs and provides a route toward computational design of improved catalysts for water oxidation.

ASSOCIATED CONTENT

Supporting Information. Tabulated values for the previously reported rate constants for catalysts in this work; details regarding spin states considered and energetic comparison between spin states; description of structure generation scheme; metrics for verifying octahedral geometry in optimized structures; a complete list of calculations which were excluded from analysis; procedure for recovery of calculations which initially did not converge to the intended result; description of calculations using functionals other than B3LYP and comparison of their results to the results of B3LYP; mathematical formulas for the calculation of each property in this work;, tabulated values for the ΔE_{vib} - ΔE_{vib}

associated with each electron transfer step for which we consider vertical ionization potential; derivation of the expected linear relationship between vertical ionization potential and reaction

rate using Marcus theory; tabulated values for each of the seven DFT properties considered in depth in this work; PCA of electron density in valence orbitals of Ru(II)-OH2 and other

intermediates; tabulated values for the electron density in valence orbitals of Ru(II)-OH₂; scatter

plots and equations for linear fits of the observed correlation between DFT properties; comparison of the reported rate constants and rate constants derived from our scaling

relationships; scatter plots and tabulated values for the deviation from scaling relationships in

catalysts with diverse electron structure; properties for 1a and the graphene analogue with an

without conformational constraints (PDF)

Structure files for the optimized geometries of all species considered in this work which pass our geometric and spin contamination criteria; complete list of calculations excluded from analysis

due to non-octahedral geometries, spin contamination, or convergence issues; energies for all

successful geometry optimizations and single point calculations in this work (ZIP)

AUTHOR INFORMATION

Corresponding Author

*email: hjkulik@mit.edu phone: 617-253-4584

Notes

The authors declare no competing financial interest.

ACKNOWLEDGMENT

The work was also supported by the Office of Naval Research under grant numbers N00014-18-

1-2434 and N00014-20-1-2150 as well as by the National Science Foundation under grant

number CBET-1846426. H.J.K. holds a Career Award at the Scientific Interface from the

Burroughs Wellcome Fund and an AAAS Marion Milligan Mason Award, which supported this

work. This work was carried out in part using computational resources from the Extreme Science

and Engineering Discovery Environment (XSEDE), which is supported by National Science

Foundation grant number ACI-1548562. The authors thank Chenru Duan, Michael G. Taylor,

and Adam H. Steeves for providing critical readings of the manuscript.

27

References

- (1) Lewis, N. S. Research Opportunities to Advance Solar Energy Utilization. *Science* **2016**, *351*, aad1920.
- (2) Janet, J. P.; Ramesh, S.; Duan, C.; Kulik, H. J. Accurate Multiobjective Design in a Space of Millions of Transition Metal Complexes with Neural-Network-Driven Efficient Global Optimization. *ACS Cent. Sci.* **2020**, *6*, 513.
- (3) Janet, J. P.; Duan, C.; Nandy, A.; Liu, F.; Kulik, H. J. Navigating Transition-Metal Chemical Space: Artificial Intelligence for First-Principles Design. *Acc. Chem. Res.* **2021,** *54*, 532.
- (4) Janet, J. P.; Chan, L.; Kulik, H. J. Accelerating Chemical Discovery with Machine Learning: Simulated Evolution of Spin Crossover Complexes with an Artificial Neural Network. *J. Phys. Chem. Lett.* **2018**, *9*, 1064.
- (5) Concepcion, J. J.; Jurss, J. W.; Templeton, J. L.; Meyer, T. J. One Site Is Enough. Catalytic Water Oxidation by [Ru(Tpy)Bpm)(Oh₂)]²⁺ and [Ru(Tpy)(Bpz)(Oh₂)]²⁺. *J. Am. Chem. Soc.* **2008**, *130*, 16462.
- (6) Zong, R.; Thummel, R. P. A New Family of Ru Complexes for Water Oxidation. *J. Am. Chem. Soc.* **2005**, *127*, 12802.
- (7) Tseng, H.-W.; Zong, R.; Muckerman, J. T.; Thummel, R. Mononuclear Ruthenium(Ii) Complexes That Catalyze Water Oxidation. *Inorg. Chem.* **2008**, *47*, 11763.
- (8) Concepcion, J. J.; Jurss, J. W.; Norris, M. R.; Chen, Z.; Templeton, J. L.; Meyer, T. J. Catalytic Water Oxidation by Single-Site Ruthenium Catalysts. *Inorg. Chem.* **2010**, *49*, 1277.
- (9) Yoshida, M.; Masaoka, S.; Sakai, K. Oxygen Evolution from Water Catalyzed by Mononuclear Ruthenium Complexes with a Triazamacrocyclic Ligand in a Facial Fashion. *Chem. Lett.* **2009**, *38*, 702.
- (10) Maji, S.; López, I.; Bozoglian, F.; Benet-Buchholz, J.; Llobet, A. Mononuclear Ruthenium–Water Oxidation Catalysts: Discerning between Electronic and Hydrogen-Bonding Effects. *Inorg. Chem.* **2013**, *52*, 3591.
- (11) Hoque, M. A.; Chowdhury, A. D.; Maji, S.; Benet-Buchholz, J.; Ertem, M. Z.; Gimbert-Suriñach, C.; Lahiri, G. K.; Llobet, A. Synthesis, Characterization, and Water Oxidation Activity of Isomeric Ru Complexes. *Inorg. Chem.* **2021**, *60*, 5791.
- (12) Wasylenko, D. J.; Ganesamoorthy, C.; Koivisto, B. D.; Henderson, M. A.; Berlinguette, C. P. Insight into Water Oxidation by Mononuclear Polypyridyl Ru Catalysts. *Inorg. Chem.* 2010, 49, 2202.
- (13) Yagi, M.; Tajima, S.; Komi, M.; Yamazaki, H. Highly Active and Tunable Catalysts for O₂ Evolution from Water Based on Mononuclear Ruthenium(Ii) Monoaquo Complexes. *Dalton Trans.* **2011**, *40*, 3802.
- (14) Watabe, S.; Tanahashi, Y.; Hirahara, M.; Yamazaki, H.; Takahashi, K.; Mohamed, E. A.; Tsubonouchi, Y.; Zahran, Z. N.; Saito, K.; Yui, T. Critical Hammett Electron-Donating Ability of Substituent Groups for Efficient Water Oxidation Catalysis by Mononuclear Ruthenium Aquo Complexes. *Inorg. Chem.* **2019**, *58*, 12716.
- (15) Duan, L.; Bozoglian, F.; Mandal, S.; Stewart, B.; Privalov, T.; Llobet, A.; Sun, L. A Molecular Ruthenium Catalyst with Water-Oxidation Activity Comparable to That of Photosystem Ii. *Nat. Chem.* **2012**, *4*, 418.

- (16) Matheu, R.; Ertem, M. Z.; Benet-Buchholz, J.; Coronado, E.; Batista, V. S.; Sala, X.; Llobet, A. Intramolecular Proton Transfer Boosts Water Oxidation Catalyzed by a Ru Complex. *J. Am. Chem. Soc.* **2015**, *137*, 10786.
- (17) Boyer, J. L.; Polyansky, D. E.; Szalda, D. J.; Zong, R.; Thummel, R. P.; Fujita, E. Effects of a Proximal Base on Water Oxidation and Proton Reduction Catalyzed by Geometric Isomers of [Ru(Tpy)(Pynap)(Oh₂)]²⁺. *Angew. Chem., Int. Ed.* **2011**, *50*, 12600.
- (18) Jacobsen, G. M.; Yang, J. Y.; Twamley, B.; Wilson, A. D.; Bullock, R. M.; DuBois, M. R.; DuBois, D. L. Hydrogen Production Using Cobalt-Based Molecular Catalysts Containing a Proton Relay in the Second Coordination Sphere. *Energy Environ. Sci.* **2008**, *1*, 167.
- (19) Kotyk, J. F. K.; Hanna, C. M.; Combs, R. L.; Ziller, J. W.; Yang, J. Y. Intramolecular Hydrogen-Bonding in a Cobalt Aqua Complex and Electrochemical Water Oxidation Activity. *Chem. Sci.* **2018**, *9*, 2750.
- (20) Yang; de Groot, H. J. M.; Buda, F. Tuning the Proton-Coupled Electron-Transfer Rate by Ligand Modification in Catalyst–Dye Supramolecular Complexes for Photocatalytic Water Splitting. *ChemSusChem* **2021**, *14*, 479.
- (21) Concepcion, J. J.; Tsai, M.-K.; Muckerman, J. T.; Meyer, T. J. Mechanism of Water Oxidation by Single-Site Ruthenium Complex Catalysts. *J. Am. Chem. Soc.* **2010**, *132*, 1545.
- (22) Duan, L.; Araujo, C. M.; Ahlquist, M. S. G.; Sun, L. Highly Efficient and Robust Molecular Ruthenium Catalysts for Water Oxidation. *Proc. Natl. Acad. Sci.* **2012**, *109*, 15584.
- (23) Duan, L.; Fischer, A.; Xu, Y.; Sun, L. Isolated Seven-Coordinate Ru(Iv) Dimer Complex with [Hohoh] Bridging Ligand as an Intermediate for Catalytic Water Oxidation. *J. Am. Chem. Soc.* **2009**, *131*, 10397.
- (24) Zhang, B.; Sun, L. Ru-Bda: Unique Molecular Water-Oxidation Catalysts with Distortion Induced Open Site and Negatively Charged Ligands. *J. Am. Chem. Soc.* **2019**, *141*, 5565.
- (25) Silva, J. L.; Unger, I.; Matias, T. A.; Franco, L. R.; Damas, G.; Costa, L. T.; Toledo, K. C. F.; Rocha, T. C. R.; de Brito, A. N.; Saak, C.-M. X-Ray Photoelectron Fingerprints of High-Valence Ruthenium—Oxo Complexes Along the Oxidation Reaction Pathway in an Aqueous Environment. *J. Phys. Chem. Lett.* **2019**, *10*, 7636.
- (26) Polyansky, D. E.; Muckerman, J. T.; Rochford, J.; Zong, R.; Thummel, R. P.; Fujita, E. Water Oxidation by a Mononuclear Ruthenium Catalyst: Characterization of the Intermediates. *J. Am. Chem. Soc.* **2011**, *133*, 14649.
- (27) Pushkar, Y.; Moonshiram, D.; Purohit, V.; Yan, L.; Alperovich, I. Spectroscopic Analysis of Catalytic Water Oxidation by [Ruⁱⁱ(Bpy)(Tpy) H2o]²⁺ Suggests That Ru(V)=O Is Not a Rate-Limiting Intermediate. *J. Am. Chem. Soc.* **2014**, *136*, 11938.
- (28) Vogiatzis, K. D.; Polynski, M. V.; Kirkland, J. K.; Townsend, J.; Hashemi, A.; Liu, C.; Pidko, E. A. Computational Approach to Molecular Catalysis by 3d Transition Metals: Challenges and Opportunities. *Chem. Rev.* **2018**, *119*, 2453.
- (29) Hughes, T. F.; Friesner, R. A. Systematic Investigation of the Catalytic Cycle of a Single Site Ruthenium Oxygen Evolving Complex Using Density Functional Theory. *J. Phys. Chem. B* **2011**, *115*, 9280.
- (30) Wang, L.-P.; Wu, Q.; Van Voorhis, T. Acid–Base Mechanism for Ruthenium Water Oxidation Catalysts. *Inorg. Chem.* **2010**, *49*, 4543.

- (31) Chen, Z.; Concepcion, J. J.; Hu, X.; Yang, W.; Hoertz, P. G.; Meyer, T. J. Concerted O Atom–Proton Transfer in the O—O Bond Forming Step in Water Oxidation. *Proc. Natl. Acad. Sci.* **2010**, *107*, 7225.
- (32) Vigara, L.; Ertem, M. Z.; Planas, N.; Bozoglian, F.; Leidel, N.; Dau, H.; Haumann, M.; Gagliardi, L.; Cramer, C. J.; Llobet, A. Experimental and Quantum Chemical Characterization of the Water Oxidation Cycle Catalysed by [Ruⁱⁱ(Damp)(Bpy)(H₂o)]²⁺. *Chem. Sci.* **2012**, *3*, 2576.
- (33) Angeles-Boza, A. M.; Ertem, M. Z.; Sarma, R.; Ibanez, C. H.; Maji, S.; Llobet, A.; Cramer, C. J.; Roth, J. P. Competitive Oxygen-18 Kinetic Isotope Effects Expose O–O Bond Formation in Water Oxidation Catalysis by Monomeric and Dimeric Ruthenium Complexes. *Chem. Sci.* **2014**, *5*, 1141.
- (34) Lin, X.; Hu, X.; Concepcion, J. J.; Chen, Z.; Liu, S.; Meyer, T. J.; Yang, W. Theoretical Study of Catalytic Mechanism for Single-Site Water Oxidation Process. *Proc. Natl. Acad. Sci.* **2012**, *109*, 15669.
- (35) Hirahara, M.; Ertem, M. Z.; Komi, M.; Yamazaki, H.; Cramer, C. J.; Yagi, M. Mechanisms of Photoisomerization and Water-Oxidation Catalysis of Mononuclear Ruthenium(Ii) Monoaquo Complexes. *Inorg. Chem.* **2013**, *52*, 6354.
- (36) Raugei, S.; DuBois, D. L.; Rousseau, R.; Chen, S.; Ho, M.-H.; Bullock, R. M.; Dupuis, M. Toward Molecular Catalysts by Computer. *Acc. Chem. Res.* **2015**, *48*, 248.
- (37) Xu, H.; Cheng, D.; Cao, D.; Zeng, X. C. A Universal Principle for a Rational Design of Single-Atom Electrocatalysts. *Nat. Catal.* **2018**, *1*, 339.
- (38) Wasylenko, D. J.; Ganesamoorthy, C.; Henderson, M. A.; Koivisto, B. D.; Osthoff, H. D.; Berlinguette, C. P. Electronic Modification of the [Ruⁱⁱ(Tpy)(Bpy)(Oh₂)]²⁺ Scaffold: Effects on Catalytic Water Oxidation. *J. Am. Chem. Soc.* **2010**, *132*, 16094.
- (39) Moonshiram, D.; Pineda-Galvan, Y.; Erdman, D.; Palenik, M.; Zong, R.; Thummel, R.; Pushkar, Y. Uncovering the Role of Oxygen Atom Transfer in Ru-Based Catalytic Water Oxidation. *J. Am. Chem. Soc.* **2016**, *138*, 15605.
- (40) Zhan, S.; Triviño, J.; Ahlquist, M. r. The Carboxylate Ligand as an Oxide Relay in Catalytic Water Oxidation. *J. Am. Chem. Soc.* **2019**, *141*, 10247.
- (41) Ertem, M. Z.; Concepcion, J. J. Oxygen Atom Transfer as an Alternative Pathway for Oxygen–Oxygen Bond Formation. *Inorg. Chem.* **2020**, *59*, 5966.
- (42) Govindarajan, N.; Tiwari, A.; Ensing, B.; Meijer, E. J. Impact of the Ligand Flexibility and Solvent on the O–O Bond Formation Step in a Highly Active Ruthenium Water Oxidation Catalyst. *Inorg. Chem.* **2018**, *57*, 13063.
- (43) Pidko, E. A. Toward the Balance between the Reductionist and Systems Approaches in Computational Catalysis: Model Versus Method Accuracy for the Description of Catalytic Systems. *ACS Catal.* **2017**, *7*, 4230.
- (44) Bergeler, M.; Simm, G. N.; Proppe, J.; Reiher, M. Heuristics-Guided Exploration of Reaction Mechanisms. *J. Chem. Theory Comput.* **2015**, *11*, 5712.
- (45) Kuliaev, P. O.; Pidko, E. A. Operando Modeling of Multicomponent Reactive Solutions in Homogeneous Catalysis: From Non-Standard Free Energies to Reaction Network Control. *ChemCatChem* **2020**, *12*, 795.
- (46) Ertem, M. Z.; Gagliardi, L.; Cramer, C. J. Quantum Chemical Characterization of the Mechanism of an Iron-Based Water Oxidation Catalyst. *Chem. Sci.* **2012**, *3*, 1293.
- (47) Gimbert-Suriñach, C.; Moonshiram, D.; Francàs, L.; Planas, N.; Bernales, V.; Bozoglian, F.; Guda, A.; Mognon, L.; López, I.; Hoque, M. A. Structural and Spectroscopic

- Characterization of Reaction Intermediates Involved in a Dinuclear Co–Hbpp Water Oxidation Catalyst. *J. Am. Chem. Soc.* **2016,** *138*, 15291.
- (48) Hu, S.; Xu, P.; Xu, R.-X.; Zheng, X. Unveiling the High Catalytic Activity of a Dinuclear Iron Complex for the Oxygen Evolution Reaction. *Inorg. Chem.* **2021**, *60*, 7297.
- (49) Besora, M.; Maseras, F. Microkinetic Modeling in Homogeneous Catalysis. *Wiley Interdiscip. Rev.: Comput. Mol. Sci.* **2018**, *8*, e1372.
- (50) Mao, Z.; Campbell, C. T. Kinetic Isotope Effects: Interpretation and Prediction Using Degrees of Rate Control. *ACS Catal.* **2020**, *10*, 4181.
- (51) Stegelmann, C.; Andreasen, A.; Campbell, C. T. Degree of Rate Control: How Much the Energies of Intermediates and Transition States Control Rates. *J. Am. Chem. Soc.* **2009**, *131*, 8077.
- (52) Kozuch, S.; Martin, J. M. L. What Makes for a Bad Catalytic Cycle? A Theoretical Study on the Suzuki– Miyaura Reaction within the Energetic Span Model. *ACS Catal.* **2011**, *1*, 246.
- (53) Kozuch, S.; Shaik, S. How to Conceptualize Catalytic Cycles? The Energetic Span Model. *Acc. Chem. Res.* **2011**, *44*, 101.
- (54) Abild-Pedersen, F.; Greeley, J.; Studt, F.; Rossmeisl, J.; Munter, T. R.; Moses, P. G.; Skulason, E.; Bligaard, T.; Nørskov, J. K. Scaling Properties of Adsorption Energies for Hydrogen-Containing Molecules on Transition-Metal Surfaces. *Phys. Rev. Lett.* **2007**, *99*, 016105.
- (55) Man, I. C.; Su, H. Y.; Calle-Vallejo, F.; Hansen, H. A.; Martínez, J. I.; Inoglu, N. G.; Kitchin, J.; Jaramillo, T. F.; Nørskov, J. K.; Rossmeisl, J. Universality in Oxygen Evolution Electrocatalysis on Oxide Surfaces. *ChemCatChem* **2011**, *3*, 1159.
- (56) Nørskov, J. K.; Bligaard, T.; Rossmeisl, J.; Christensen, C. H. Towards the Computational Design of Solid Catalysts. *Nat. Chem.* **2009**, *1*, 37.
- (57) Latimer, A. A.; Kulkarni, A. R.; Aljama, H.; Montoya, J. H.; Yoo, J. S.; Tsai, C.; Abild-Pedersen, F.; Studt, F.; Nørskov, J. K. Understanding Trends in C–H Bond Activation in Heterogeneous Catalysis. *Nat. Mater.* **2017**, *16*, 225.
- (58) Liao, P.; Getman, R. B.; Snurr, R. Q. Optimizing Open Iron Sites in Metal–Organic Frameworks for Ethane Oxidation: A First-Principles Study. *ACS Appl. Mater. Interfaces* **2017**, *9*, 33484.
- (59) Yang, X.-F.; Wang, A.; Qiao, B.; Li, J.; Liu, J.; Zhang, T. Single-Atom Catalysts: A New Frontier in Heterogeneous Catalysis. *Acc. Chem. Res.* **2013**, *46*, 1740.
- (60) Flytzani-Stephanopoulos, M. Gold Atoms Stabilized on Various Supports Catalyze the Water–Gas Shift Reaction. *Acc. Chem. Res.* **2014**, *47*, 783.
- (61) Wodrich, M. D.; Sawatlon, B.; Busch, M.; Corminboeuf, C. The Genesis of Molecular Volcano Plots. *Acc. Chem. Res.* **2021**, *54*, 1107.
- (62) Cordova, M.; Wodrich, M. D.; Meyer, B.; Sawatlon, B.; Corminboeuf, C. Data-Driven Advancement of Homogeneous Nickel Catalyst Activity for Aryl Ether Cleavage. *ACS Catal.* **2020**, *10*, 7021.
- (63) Busch, M.; Wodrich, M. D.; Corminboeuf, C. Linear Scaling Relationships and Volcano Plots in Homogeneous Catalysis–Revisiting the Suzuki Reaction. *Chem. Sci.* **2015**, *6*, 6754.
- (64) Deshpande, S.; Kitchin, J. R.; Viswanathan, V. Quantifying Uncertainty in Activity Volcano Relationships for Oxygen Reduction Reaction. *ACS Catal.* **2016**, *6*, 5251.

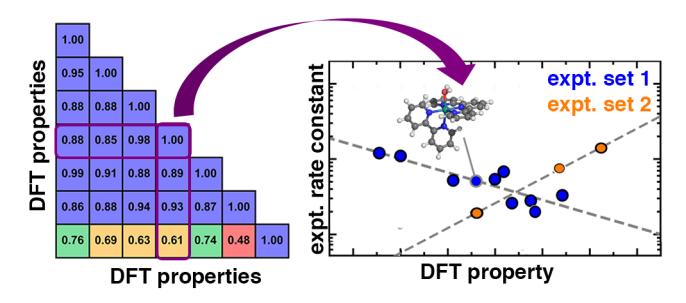
- (65) Mori-Sánchez, P.; Cohen, A. J.; Yang, W. Many-Electron Self-Interaction Error in Approximate Density Functionals. *J. Chem. Phys.* **2006**, *125*, 201102.
- (66) Ruzsinszky, A.; Perdew, J. P.; Csonka, G. I.; Vydrov, O. A.; Scuseria, G. E. Density Functionals That Are One-and Two-Are Not Always Many-Electron Self-Interaction-Free, as Shown for H₂⁺, He₂⁺, Lih⁺, and Ne₂⁺. *J. Chem. Phys.* **2007**, *126*, 104102.
- (67) Haunschild, R.; Henderson, T. M.; Jimenez-Hoyos, C. A.; Scuseria, G. E. Many-Electron Self-Interaction and Spin Polarization Errors in Local Hybrid Density Functionals. *J. Chem. Phys.* **2010**, *133*, 134116.
- (68) Cohen, A. J.; Mori-Sánchez, P.; Yang, W. Insights into Current Limitations of Density Functional Theory. *Science* **2008**, *321*, 792.
- (69) Schmidt, T.; Kümmel, S. One-and Many-Electron Self-Interaction Error in Local and Global Hybrid Functionals. *Phys. Rev. B* **2016**, *93*, 165120.
- (70) Mori-Sánchez, P.; Cohen, A. J.; Yang, W. Localization and Delocalization Errors in Density Functional Theory and Implications for Band-Gap Prediction. *Phys. Rev. Lett.* **2008**, *100*, 146401.
- (71) Kulik, H. J. Perspective: Treating Electron over-Delocalization with the Dft+U Method. *J. Chem. Phys.* **2015**, *142*, 240901.
- (72) Cramer, C. J.; Truhlar, D. G. Density Functional Theory for Transition Metals and Transition Metal Chemistry. *Phys. Chem. Chem. Phys.* **2009**, *11*, 10757.
- (73) Craig, M.; Garcia-Melchor, M. High-Throughput Screening and Rational Design to Drive Discovery in Molecular Water Oxidation Catalysis. *ChemRxiv* **2021**.
- (74) Craig, M. J.; Coulter, G.; Dolan, E.; Soriano-López, J.; Mates-Torres, E.; Schmitt, W.; García-Melchor, M. Universal Scaling Relations for the Rational Design of Molecular Water Oxidation Catalysts with near-Zero Overpotential. *Nat. Commun.* **2019**, *10*, 1.
- (75) Gani, T. Z. H.; Kulik, H. J. Understanding and Breaking Scaling Relations in Single-Site Catalysis: Methane-to-Methanol Conversion by Fe(Iv)=O. *ACS Catal.* **2018**, *8*, 975.
- (76) Nandy, A.; Kulik, H. J. Why Conventional Design Rules for C-H Activation Fail for Open Shell Transition Metal Catalysts. *ACS Catal.* **2020**, *10*, 15033.
- (77) Nandy, A.; Zhu, J.; Janet, J. P.; Duan, C.; Getman, R. B.; Kulik, H. J. Machine Learning Accelerates the Discovery of Design Rules and Exceptions in Stable Metal-Oxo Intermediate Formation. *ACS Catal.* **2019**, *9*, 8243.
- (78) Andrikopoulos, P. C.; Michel, C.; Chouzier, S.; Sautet, P. In Silico Screening of Iron-Oxo Catalysts for Ch Bond Cleavage. *ACS Catal.* **2015**, *5*, 2490.
- (79) Wodrich, M. D.; Busch, M.; Corminboeuf, C. Accessing and Predicting the Kinetic Profiles of Homogeneous Catalysts from Volcano Plots. *Chem. Sci.* **2016**, *7*, 5723.
- (80) Harper, D.; Kulik, H. Computational Scaling Relationships Predict Experimental Activity and Rate Limiting Behavior in Homogenous Water Oxidation. *ChemRxiv:* https://doi.org/10.33774/chemrxiv-2021-vjbh3 2021.
- (81) Petachem. Http://Www.Petachem.Com. (Accessed October 27, 2019).
- (82) Ufimtsev, I. S.; Martinez, T. J. Quantum Chemistry on Graphical Processing Units. 3. Analytical Energy Gradients, Geometry Optimization, and First Principles Molecular Dynamics. *J. Chem. Theory Comput.* **2009**, *5*, 2619.
- (83) Lee, C.; Yang, W.; Parr, R. G. Development of the Colle-Salvetti Correlation-Energy Formula into a Functional of the Electron Density. *Phys. Rev. B* **1988**, *37*, 785.
- (84) Becke, A. D. Density-Functional Thermochemistry. Iii. The Role of Exact Exchange. *J. Chem. Phys.* **1993**, *98*, 5648.

- (85) Stephens, P. J.; Devlin, F. J.; Chabalowski, C. F.; Frisch, M. J. Ab Initio Calculation of Vibrational Absorption and Circular Dichroism Spectra Using Density Functional Force Fields. *J. Phys. Chem.* **1994**, *98*, 11623.
- (86) Hay, P. J.; Wadt, W. R. Ab Initio Effective Core Potentials for Molecular Calculations. Potentials for the Transition Metal Atoms Sc to Hg. *J. Chem. Phys.* **1985**, *82*, 270.
- (87) Ditchfield, R.; Hehre, W. J.; Pople, J. A. Self-Consistent Molecular-Orbital Methods. Ix. An Extended Gaussian-Type Basis for Molecular-Orbital Studies of Organic Molecules. *J. Chem. Phys.* **1971**, *54*, 724.
- (88) Duan, C.; Chen, S.; Taylor, M. G.; Liu, F.; Kulik, H. J. Machine Learning to Tame Divergent Density Functional Approximations: A New Path to Consensus Materials Design Principles. *Chem. Sci.* **2021**, *just accepted*.
- (89) Yang, X.; Baik, M.-H. The Mechanism of Water Oxidation Catalysis Promoted by [Tpyru(Iv)=O]213+: A Computational Study. *J. Am. Chem. Soc.* **2008**, *130*, 16231.
- (90) Lange, A. W.; Herbert, J. M. A Smooth, Nonsingular, and Faithful Discretization Scheme for Polarizable Continuum Models: The Switching/Gaussian Approach. *J. Chem. Phys.* **2010**, *133*, 244111.
- (91) York, D. M.; Karplus, M. A Smooth Solvation Potential Based on the Conductor-Like Screening Model. *J. Phys. Chem. A* **1999**, *103*, 11060.
- (92) Liu, F.; Luehr, N.; Kulik, H. J.; Martínez, T. J. Quantum Chemistry for Solvated Molecules on Graphical Processing Units Using Polarizable Continuum Models. *J. Chem. Theory Comput.* **2015**, *11*, 3131.
- (93) Liu, F.; Sanchez, D. M.; Kulik, H. J.; Martínez, T. J. Exploiting Graphical Processing Units to Enable Quantum Chemistry Calculation of Large Solvated Molecules with Conductor-Like Polarizable Continuum Models. *Int. J. Quantum Chem.* **2019**, *119*, e25760.
- (94) Saunders, V. R.; Hillier, I. H. A "Level-Shifting" Method for Converging Closed Shell Hartree-Fock Wave Functions. *Int. J. Quantum Chem.* **1973,** *7*, 699.
- (95) Wang, L.-P.; Song, C. Geometry Optimization Made Simple with Translation and Rotation Coordinates. *J. Chem. Phys.* **2016**, *144*, 214108.
- (96) Gillespie, A. M.; Morello, G. R.; White, D. P. De Novo Ligand Design: Understanding Stereoselective Olefin Binding to [(H5-C5h5)Re(No)(Pph3)]+ with Molecular Mechanics, Semiempirical Quantum Mechanics, and Density Functional Theory. *Organometallics* **2002**, *21*, 3913.
- (97) Buda, C.; Burt, S. K.; Cundari, T. R.; Shenkin, P. S. De Novo Structural Prediction of Transition Metal Complexes: Application to Technetium. *Inorg. Chem.* **2002**, *41*, 2060.
- (98) Nandy, A.; Duan, C.; Taylor, M. G.; Liu, F.; Steeves, A. H.; Kulik, H. J. Computational Discovery of Transition-Metal Complexes: From High-Throughput Screening to Machine Learning. *Chem. Rev.* **2021**, *121*, 9927.
- (99) Menzel, J. P.; Kloppenburg, M.; Belić, J.; de Groot, H. J. M.; Visscher, L.; Buda, F. Efficient Workflow for the Investigation of the Catalytic Cycle of Water Oxidation Catalysts: Combining Gfn-Xtb and Density Functional Theory. *J. Comput. Chem.* **2021**, 42, 1885.
- (100) Ioannidis, E. I.; Gani, T. Z. H.; Kulik, H. J. Molsimplify: A Toolkit for Automating Discovery in Inorganic Chemistry. *J. Comput. Chem.* **2016**, *37*, 2106.
- (101) Molsimplify Documentation. http://molsimplify.mit.edu. (Accessed March 3, 2021).

- (102) Group, K. Molsimplify & Molsimplify Automatic Design. https://github.com/hjkgrp/molsimplify. (Accessed March 3, 2021).
- (103) O'Boyle, N. M.; Banck, M.; James, C. A.; Morley, C.; Vandermeersch, T.; Hutchison, G. R. Open Babel: An Open Chemical Toolbox. *J. Cheminf.* **2011**, *3*, 33.
- (104) O'Boyle, N. M.; Morley, C.; Hutchison, G. R. Pybel: A Python Wrapper for the Open Babel Cheminformatics Toolkit. *Chem. Cent. J.* **2008**, *2*, 5.
- (105) Nandy, A.; Duan, C.; Janet, J. P.; Gugler, S.; Kulik, H. J. Strategies and Software for Machine Learning Accelerated Discovery in Transition Metal Chemistry. *Ind. Eng. Chem. Res.* 2018, 57, 13973.
- (106) Ioannidis, E. I.; Kulik, H. J. Ligand-Field-Dependent Behavior of Meta-Gga Exchange in Transition-Metal Complex Spin-State Ordering. *J. Phys. Chem. A* **2017**, *121*, 874.
- (107) Yanai, T.; Tew, D. P.; Handy, N. C. A New Hybrid Exchange—Correlation Functional Using the Coulomb-Attenuating Method (Cam-B3lyp). *Chem. Phys. Lett.* **2004**, *393*, 51.
- (108) Chai, J.-D.; Head-Gordon, M. Systematic Optimization of Long-Range Corrected Hybrid Density Functionals. *J. Chem. Phys.* **2008**, *128*, 084106.
- (109) Rohrdanz, M. A.; Martins, K. M.; Herbert, J. M. A Long-Range-Corrected Density Functional That Performs Well for Both Ground-State Properties and Time-Dependent Density Functional Theory Excitation Energies, Including Charge-Transfer Excited States. *J. Chem. Phys.* **2009**, *130*, 054112.
- (110) Gorantla, K. R.; Mallik, B. S. Mechanism and Electronic Perspective of Oxygen Evolution Reactions Catalyzed by [Fe(Otf)2(Bpbp)]. *J. Phys. Chem. C* **2021**, *125*, 1313.
- (111) Gagliardi, C. J.; Vannucci, A. K.; Concepcion, J. J.; Chen, Z.; Meyer, T. J. The Role of Proton Coupled Electron Transfer in Water Oxidation. *Energy Environ. Sci.* **2012**, *5*, 7704.
- (112) Fahmida, K.; Sonalika, A.; Ganesh, S. Reaction Mechanism of the Ceric Oxidation of Benzohydroxamic Acid with Different Acid Medium. *Res. J. Chem. Environ.* **2013**, *17*, 5.
- (113) Koper, M. T. M. Analysis of Electrocatalytic Reaction Schemes: Distinction between Rate-Determining and Potential-Determining Steps. *Journal of Solid State Electrochemistry* **2013**, *17*, 339.
- (114) de Ruiter, J. M.; Purchase, R. L.; Monti, A.; van der Ham, C. J. M.; Gullo, M. P.; Joya, K. S.; D'Angelantonio, M.; Barbieri, A.; Hetterscheid, D. G. H.; de Groot, H. J. M.et al. Electrochemical and Spectroscopic Study of Mononuclear Ruthenium Water Oxidation Catalysts: A Combined Experimental and Theoretical Investigation. *ACS Catal.* **2016**, *6*, 7340.
- (115) Bell, R. P. The Theory of Reactions Involving Proton Transfers. *Proc. R. Soc. London, Ser. A* **1936,** *154*, 414.
- (116) Evans, M. G.; Polanyi, M. Inertia and Driving Force of Chemical Reactions. *Trans. Faraday Soc.* **1938,** *34*, 11.
- (117) Marcus, R. A.; Sutin, N. Electron Transfers in Chemistry and Biology. *Biochim. Biophys. Acta, Rev. Bioenerg.* **1985**, *811*, 265.
- (118) Betley, T. A.; Wu, Q.; Van Voorhis, T.; Nocera, D. G. Electronic Design Criteria for O-O Bond Formation Via Metal-Oxo Complexes. *Inorg. Chem.* **2008**, *47*, 1849.
- (119) Sit, P. H.-L.; Car, R.; Cohen, M. H.; Selloni, A. Simple, Unambiguous Theoretical Approach to Oxidation State Determination Via First-Principles Calculations. *Inorg. Chem.* **2011**, *50*, 10259.

- (120) Bucci, A.; Menendez Rodriguez, G.; Bellachioma, G.; Zuccaccia, C.; Poater, A.; Cavallo, L.; Macchioni, A. An Alternative Reaction Pathway for Iridium-Catalyzed Water Oxidation Driven by Cerium Ammonium Nitrate (Can). *ACS Catal.* **2016**, *6*, 4559.
- (121) Marshall-Roth, T.; Libretto, N. J.; Wrobel, A. T.; Anderton, K. J.; Pegis, M. L.; Ricke, N. D.; Van Voorhis, T.; Miller, J. T.; Surendranath, Y. A Pyridinic Fe-N-4 Macrocycle Models the Active Sites in Fe/N-Doped Carbon Electrocatalysts. *Nat. Commun.* **2020**, *11*, 7343.
- (122) Lee, W. H.; Ko, Y.-J.; Kim, J.-Y.; Min, B. K.; Hwang, Y. J.; Oh, H.-S. Single-Atom Catalysts for the Oxygen Evolution Reaction: Recent Developments and Future Perspectives. *Chem. Commun.* **2020,** *56*, 12687.
- (123) Evangelisti, F.; Güttinger, R.; Moré, R.; Luber, S.; Patzke, G. R. Closer to Photosystem Ii: A Co4o4 Cubane Catalyst with Flexible Ligand Architecture. *J. Am. Chem. Soc.* **2013**, *135*, 18734.
- (124) Cao, L.; Luo, Q.; Chen, J.; Wang, L.; Lin, Y.; Wang, H.; Liu, X.; Shen, X.; Zhang, W.; Liu, W. Dynamic Oxygen Adsorption on Single-Atomic Ruthenium Catalyst with High Performance for Acidic Oxygen Evolution Reaction. *Nat. Commun.* **2019**, *10*, 1.
- (125) Zhang, L.; Jia, Y.; Gao, G.; Yan, X.; Chen, N.; Chen, J.; Soo, M. T.; Wood, B.; Yang, D.; Du, A. Graphene Defects Trap Atomic Ni Species for Hydrogen and Oxygen Evolution Reactions. *Chem* **2018**, *4*, 285.
- (126) Guan, J.; Duan, Z.; Zhang, F.; Kelly, S. D.; Si, R.; Dupuis, M.; Huang, Q.; Chen, J. Q.; Tang, C.; Li, C. Water Oxidation on a Mononuclear Manganese Heterogeneous Catalyst. *Nat. Catal.* **2018**, *1*, 870.
- (127) Zheng, Y.; Jiao, Y.; Zhu, Y.; Cai, Q.; Vasileff, A.; Li, L. H.; Han, Y.; Chen, Y.; Qiao, S.-Z. Molecule-Level G-C₃n₄ Coordinated Transition Metals as a New Class of Electrocatalysts for Oxygen Electrode Reactions. *J. Am. Chem. Soc.* **2017**, *139*, 3336.

For Table of Contents Only



Computational descriptors explain differences in experimentally observed water oxidation catalyst activity with change in conditions and ligand identity.